

Neuronal activity enhances tau propagation and tau pathology *in vivo*

Jessica W Wu¹, Syed A Hussaini^{1,2}, Isle M Bastille¹, Gustavo A Rodriguez¹, Ana Mrejeru³, Kelly Rilett¹, David W Sanders⁴, Casey Cook⁵, Hongjun Fu¹, Rick A C M Boonen¹, Mathieu Herman¹, Eden Nahmani¹, Sheina Emrani¹, Y Helen Figueroa¹, Marc I Diamond⁴, Catherine L Clelland¹, Selina Wray⁶ & Karen E Duff^{1,2,7}

Tau protein can transfer between neurons transneuronally and trans-synaptically, which is thought to explain the progressive spread of tauopathy observed in the brain of patients with Alzheimer's disease. Here we show that physiological tau released from donor cells can transfer to recipient cells via the medium, suggesting that at least one mechanism by which tau can transfer is via the extracellular space. Neuronal activity has been shown to regulate tau secretion, but its effect on tau pathology is unknown. Using optogenetic and chemogenetic approaches, we found that increased neuronal activity stimulates the release of tau *in vitro* and enhances tau pathology *in vivo*. These data have implications for disease pathogenesis and therapeutic strategies for Alzheimer's disease and other tauopathies.

Misfolded, hyperphosphorylated forms of the microtubule stabilizing protein tau accumulate as neurofibrillary tangles in Alzheimer's disease (AD). In the earliest stages of the disease, tau is found in the somatodendritic compartment of neurons located in the transentorhinal cortex (EC)¹. Tau pathology spreads medially and worsens in the EC; it then accumulates in limbic areas, followed by neocortical areas in a pattern that suggests spread along neuroanatomical connections¹. Various mouse models have been created to replicate the progressive spread of pathology, including those using regional promoters^{2–4}, inoculation models^{5–9} and viral models^{10,11}, and it is now well established that tau has the capability to transfer between cells both *in vivo* and *in vitro*^{8,12}. Two hypotheses have been proposed to explain the propagation of tau pathology. First, intracellular tau could transfer directly between cells through physical connections such as tunneling nanotubes, as shown *in vitro* for misfolded proteins such as prions¹³. Alternatively, tau could be released into the extracellular space, either as free tau or in vesicles such as exosomes^{14–16} or ectosomes¹⁷. Data showing that tau is present in the cerebrospinal fluid and interstitial fluid (ISF) of tau transgenic mouse lines^{18–20} and the cerebrospinal fluid and ISF of AD brains²¹, together with data showing tau is released into the medium of cultured neurons²², support the second hypothesis. Although there is strong evidence that tau is released from cells, the competence of extracellular tau generated *in vitro* by neurons to contribute to cell-to-cell propagation has not been tested. Using physiologically relevant culture systems, including human induced pluripotent stem cells (iPSCs), we have shown that tau released from donor cells into the medium can be internalized by recipient cells, where it can stimulate the generation of more

aberrant tau. Furthermore, using a tripartite microfluidic system, we have shown that the aberrant tau generated in recipients can be passed to subsequent recipient cells, indicating true propagation.

The mechanism by which tau can be released from neurons is unknown, but its release can be stimulated by enhanced neuronal activity both *in vitro*²² and *in vivo*²³. As cells in the AD¹³ brain could be hyperexcitable^{24–28}, the impact of enhanced neuronal activity on tauopathy is of significant interest. Using sophisticated optogenetic and chemogenetic manipulations, we have demonstrated that increasing neuronal activity can not only enhance release and transfer of tau *in vitro*, but also exacerbate tau pathology *in vivo*.

RESULTS

Endogenously generated tau transfers from cell to cell

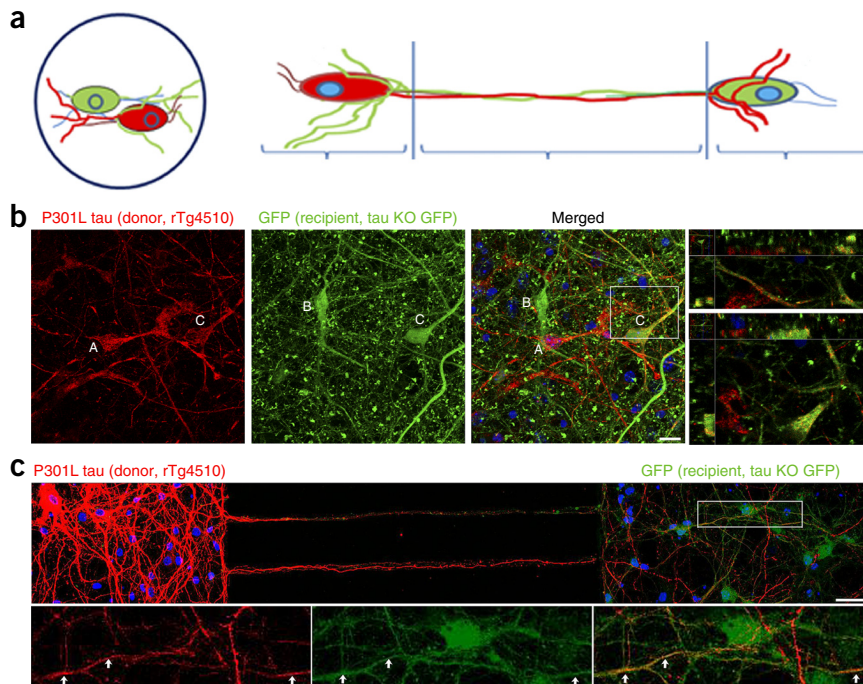
To examine whether physiologically relevant, human tau (hTau) can transfer between neurons, we cultured neurons derived from a transgenic mouse line expressing hTau P301L (line rTg4510, 'donor')²⁹ with neurons from a *MAPT*^{-/-}:*GFP* (tau knockout-GFP line, 'recipient')³⁰ (Fig. 1a). After 2 weeks, hTau accumulated in the cytosol and neurites of recipient cells grown on plates (Fig. 1b) and in microfluidic chambers (Fig. 1c). To determine whether highly aggregated forms of tau have a greater propensity for neuron-to-neuron transfer, we compared the effects of two types of seeds on tau transfer: clone 9 seeds, which have been shown to induce the formation of robust aggregates of tau, or clone 1 seeds, which do not induce the formation of aggregates of tau⁸. In this experiment, the tau that is expressed in donor cells was fluorescently tagged (with repeat domain P301S-YFP) so that it could be directly visualized in the recipients. Lysate containing clone 1 seeds did not readily

¹Taub Institute, Columbia University Medical Center, New York, New York, USA. ²Department of Pathology and Cell Biology, Columbia University Medical Center, New York, New York, USA. ³Department of Neurology, Columbia University Medical Center, New York, New York, USA. ⁴Center for Alzheimer's and Neurodegenerative Diseases, University of Texas Southwestern Medical Center, Dallas, Texas, USA. ⁵Department of Neuroscience, Mayo Clinic, Jacksonville, Florida, USA. ⁶Department of Molecular Neuroscience, Institute of Neurology, University College, London, UK. ⁷Department of Integrative Neuroscience, New York State Psychiatric Institute, New York, New York, USA. Correspondence should be addressed to K.E.D. (ked2115@columbia.edu).

Received 17 December 2015; accepted 18 May 2016; published online 20 June 2016; doi:10.1038/nn.4328

Figure 1 Endogenously generated hTau can transfer from cell to cell. **(a)** We cocultured neurons on coverslips (left) and in microfluidic chamber devices (right). Cocultures of mutant hTau-expressing neurons (red, from rTg4510 line; cell A) and recipient tau knockout (KO) neurons (green, from tau KO line; cells B and C). **(b)** hTau in recipient tau KO cell (cell C, yellow) on coverslip (enlarged images, cell C in xz perspective) and **(c)** in microfluidic chambers (yellow, arrows). Scale bars, 10 μ m in **b** and 50 μ m in **c**; rectangles indicate areas enlarged at right (**b**) or bottom (**c**). Images are representative of four neuronal cultures.

induce any obvious aggregates in donor cells even after extensive culturing (20 days *in vitro* (DIV)). In contrast, when lysate containing clone 9 seeds was added, YFP-tagged endogenous tau began forming perinuclear aggregates in cells after 5 DIV. The number of cells forming tau aggregates increased dramatically after 20 DIV, demonstrating that template-induced tau aggregation is time-dependent (**Fig. 2a**). To assess whether induced tau aggregates were transferred to recipients, seeded donor cells were cultured with mCherry-expressing recipient neurons. YFP-tau from clone-9-seeded cells, but not clone-1-seeded cells, readily accumulated in the cytoplasm of recipient cells (**Fig. 2b,c**). Controls included neurons expressing YFP but no tau, cultured with neurons expressing mCherry. In the absence of tau, no transfer of YFP or mCherry was seen (data not shown).



To test whether aggregate formation can be induced in downstream cells, we turned to bi- and tripartite microfluidic chamber devices (**Fig. 3a,d**). The chambers allow axons from one compartment to grow through microchannels into an adjacent compartment while isolating cell bodies and dendrites in one compartment. The fluidically isolated microenvironment in each chamber allowed the delivery of agents such as seeds to one cell population without them crossing over into the next compartment^{9,31}. Repeat-domain (RD) P301S-YFP neurons were grown in each chamber. Unseeded tau-expressing cells did not form visible aggregates (**Fig. 3b**), but adding clone-9-seeded lysate to cells in the first compartment (population 1) induced endogenous YFP-tagged tau to form aggregates (**Fig. 3c**). Endogenous tau in neurons grown in the second compartment (population 2) formed aggregates after 12–15 DIV in response to aggregated tau being formed and transferred from population 1 (**Fig. 3c**). To confirm true cell-to-cell tau propagation, we used tripartite microfluidic chambers and

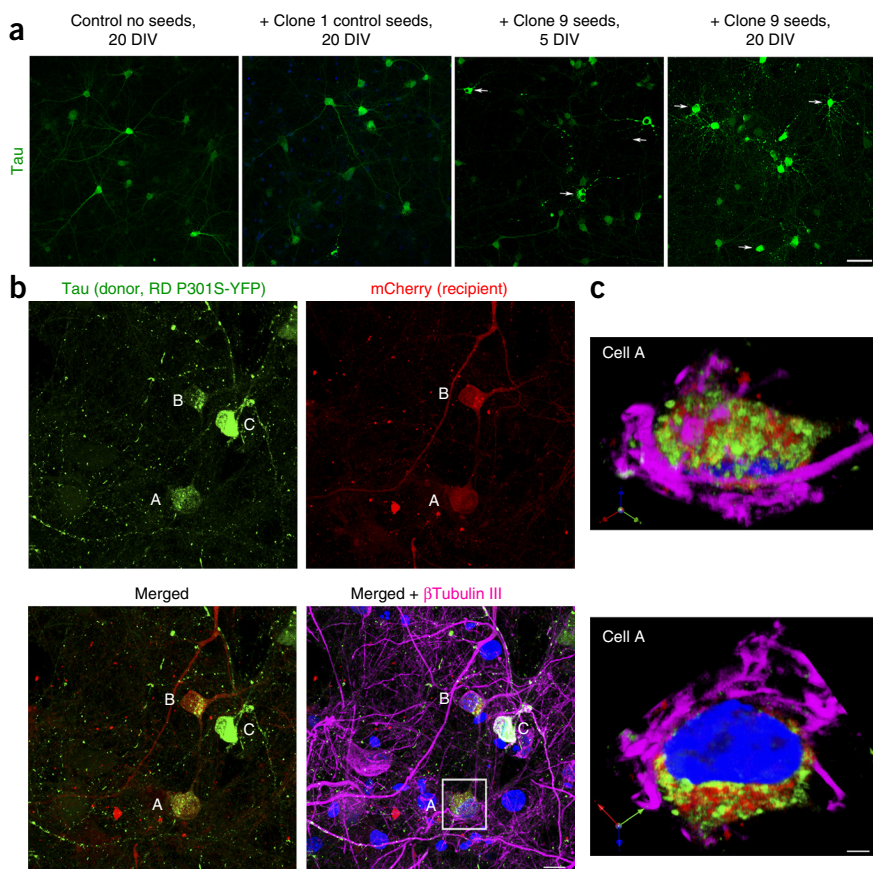


Figure 2 Endogenously generated hTau aggregates can transfer from cell to cell. **(a)** Tau repeat domain (RD)-expressing neurons (hTau RD P301S-YFP, green) do not readily form aggregates when exposed to PBS or clone 1 lysate after 20 DIV. Clone 9 lysate-seeded tau cells start forming aggregates (arrows) at 5 DIV and increase aggregate formation after 20 DIV. Scale bar, 50 μ m. **(b)** Seeded tau RD P301S-YFP aggregates (green) transferred to recipient cells (mCherry, red) (cells A and B, yellow). Scale bar, 10 μ m. **(c)** Enlarged xyz (arrows) view of cell A showing transferred tau in the cytoplasm of the cell. Images are representative of four neuronal cultures. Scale bar, 2 μ m.

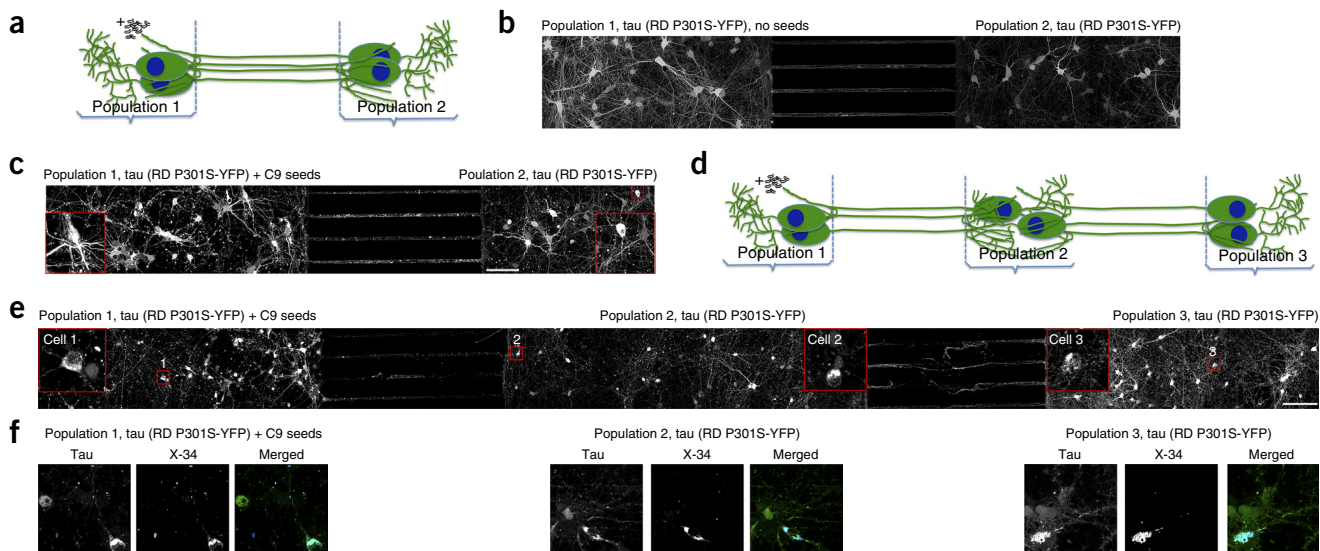
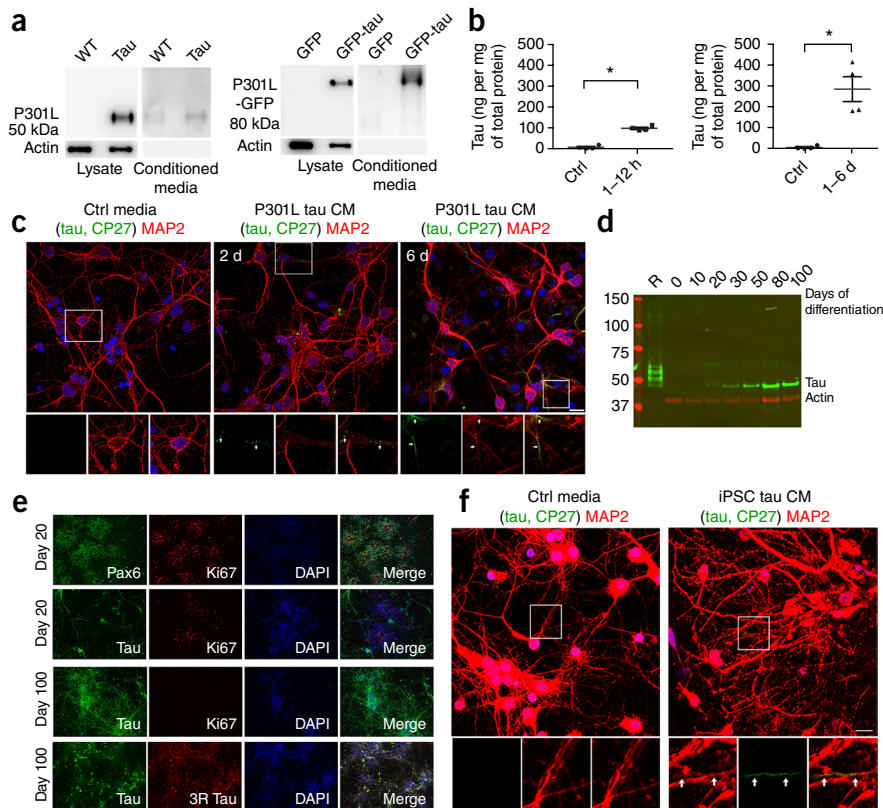


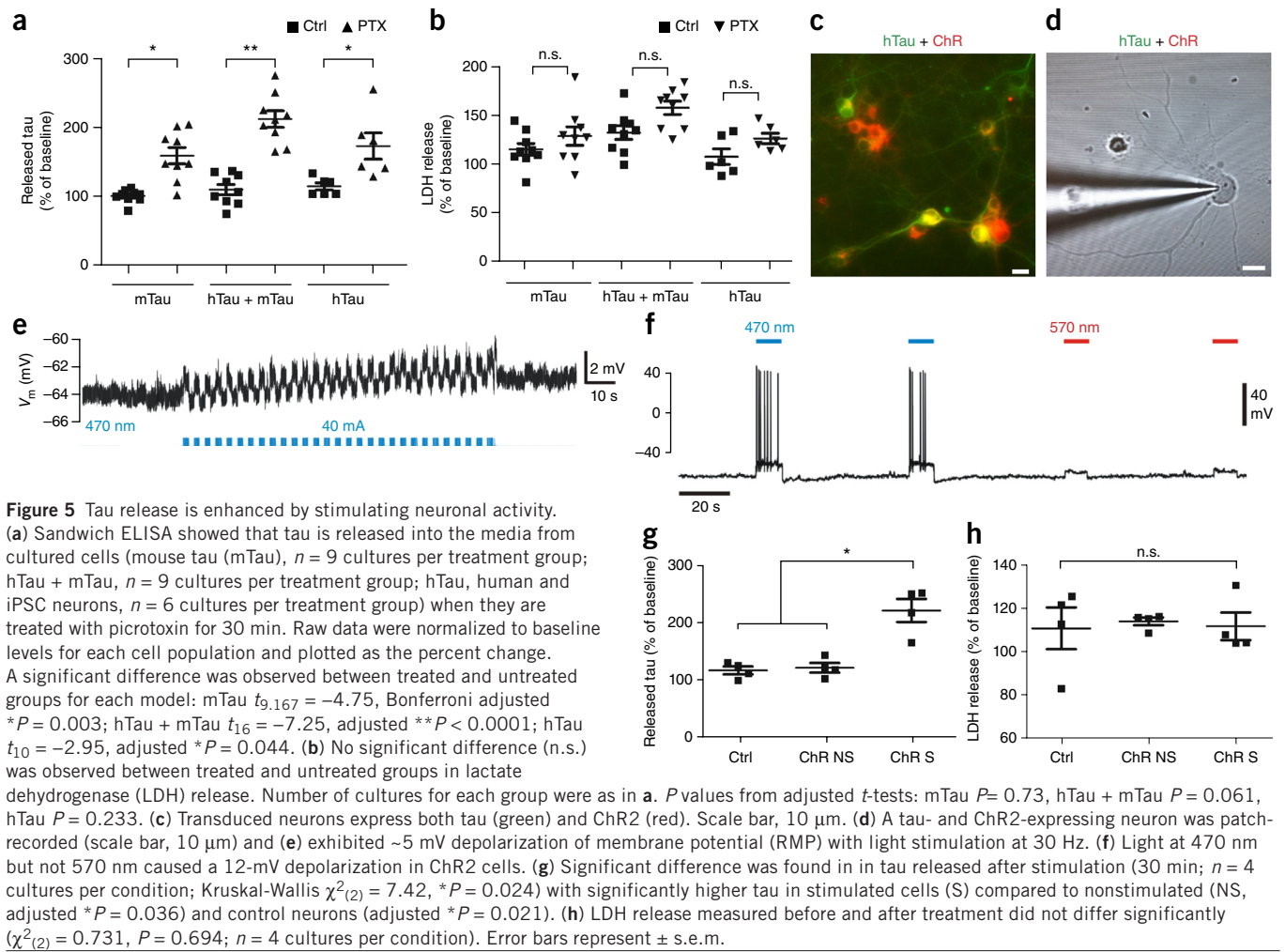
Figure 3 Seed-induced tau pathology propagates from cell to cell. (a) Cocultures in microfluidic devices with two chambers with tau seeds (black objects) added. (b) Unseeded tau-expressing cells (populations 1 and 2) grown in bipartite chamber device do not form visible aggregates. (c) Seeding population 1 with clone 9 (C9) lysate triggered endogenous tau to form aggregates in population 1 and population 2. Images are representative of three cultures. Red boxes, enlarged images. (d) Cocultures in three-chambered microfluidic devices. (e) Pathology propagated from population 1 cells to population 3 cells grown in tripartite chambers. Red boxes, enlarged images of cells 1, 2 and 3 showing tau-aggregate-containing neurons from populations 1, 2, and 3, respectively. Images are representative of two cultures. (f) Tau aggregate-containing neurons from another culture grown in a tripartite chamber showing cells from populations 1, 2 and 3 stained with X-34. Scale bars, 100 μm in **b,c,e**; 10 μm in **f**.

added seed-containing lysate only to neurons in the first compartment (population 1). We then examined whether tau aggregates could propagate not only to the second compartment (population 2), but also

to the third compartment (population 3) (Fig. 3d). After 15–18 DIV, tau aggregates were found in some population 3 neurons (Fig. 3e). The misfolded conformation of these aggregates was confirmed by

Figure 4 Tau from mouse primary neurons and human iPSCs can transfer via the extracellular medium. (a) Lysate and conditioned media from wild-type (WT), rTg4510 (Tau), GFP and P301L-GFP transduced primary neurons, labeled with tau antibody TauC. Actin was used as a loading control. (Full-length blots shown in **Supplementary Fig. 4**.) (b) Enzyme-linked immunosorbent assay (ELISA) using tau-specific antibodies showing uptake of tau from media by tau KO cells. Compared to controls ($n = 4$ cultures), tau was significantly higher in neurons after 1–12 h of incubation with tau-conditioned media ($n = 6$, $z = -2.558$, adjusted $*P = 0.021$; left), and also within 6 d of incubation ($n = 4$, $z = -2.309$, adjusted $*P = 0.042$; right). Error bars represent \pm s.e.m. (c) Neurons (wild type, WT), incubated with conditioned media (CM) from WT neurons (ctrl media), or with rTg4510 conditioned media for 2 and 6 d, labeled with tau-antibody (CP27, green), anti-MAP2 (red) and DAPI (blue). Insets show tau (arrows) in cell bodies and neurites. Scale bar, 10 μm . (d) Total tau in human iPSC neuron lysates. Recombinant tau ladder (R) separates in the following order of decreasing molecular weight: 2N4R, 2N3R, 1N4R, 1N3R, 0N4R, 0N3R. The single tau band corresponds to the 0N3R isoform. (e) iPSC cultures immunolabeled for the early forebrain marker Pax6 or tau (green) and Ki67 (red); tau was only expressed in postmitotic neurons. By day 100 of differentiation, the majority of the cells in culture were immunoreactive for total tau (green) and 0N3R (3R) tau (RD3, red). Scale bar, 100 μm . (f) Wild-type neurons treated for 6 d with control media (left) or tau conditioned media collected from iPSC neurons (right), stained with antibodies (anti-tau, CP27, green; anti-MAP2, red) and DAPI (blue). Enlarged insets show tau (green) accumulating inside neurites (yellow). Scale bar, 10 μm .





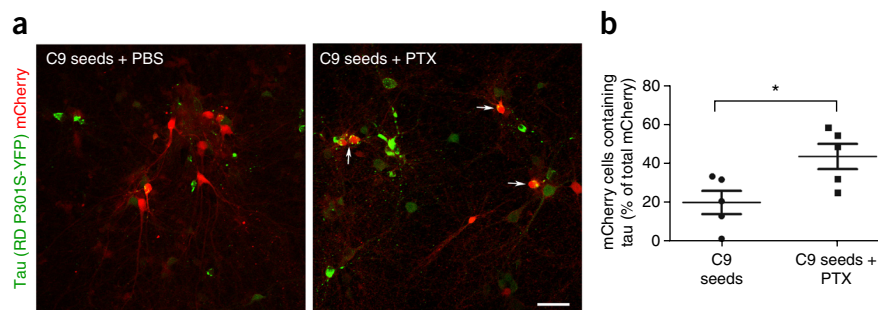
staining with X-34, a fluorescent Congo red derivative that binds to neurofibrillary tangles (Fig. 3f)³².

Tau transfers to recipients via the extracellular medium

We next examined whether tau transfer from donor neurons to recipient neurons requires cell-to-cell contact, or whether tau released into the extracellular fluid is sufficient. Lysate and conditioned medium were collected from primary neurons overexpressing tau or from neurons infected with tau virus, and tau was immunoprecipitated using an hTau-specific antibody and analyzed by western blot. Tau was detected in the media of both cell models (Fig. 4a). Actin was present in lysates but absent in medium fraction, demonstrating that the media were not contaminated with cell debris. Next, we incubated wild-type recipient neurons with conditioned media from hTau-expressing donor cells for incubation periods of 1 h, 6 h, 12 h, 1 d or 6 d. Recipient neurons accumulated tau within hours and had a substantial amount of tau accumulation by 6 d (Fig. 4b). Immunofluorescence staining revealed that the internalized tau initially accumulated in discrete puncta in the cytosol and dendrites of recipient neurons after 2 d (Fig. 4c), but it later appeared more diffusely distributed in cell bodies and neurites (Fig. 4c). To confirm that tau was released into the medium from cells expressing it at physiological levels, we examined iPSCs that were differentiated into cortical neurons by dual SMAD inhibition followed by an extended period of *in vitro* corticogenesis (Fig. 4d,e)³³. SMADs are intracellular transcription factors that transduce

extracellular transforming growth factors (TGF- β) that are important for cell growth and differentiation. *In vitro* corticogenesis using this method has been shown to take up to 90 d, producing all classes of glutamatergic projection neurons that make mature, functional synapses capable of firing repetitive action potentials³⁴. Immunoblotting of whole-cell lysates at time points throughout differentiation (Fig. 4d) showed a single band that was immunoreactive for tau at all time points from day 20 onwards. Comparison with a recombinant tau ladder confirmed this was the 0N3R tau isoform, consistent with previous reports that iPSC-neurons mainly express fetal tau isoform and not the adult isoform ratio of equivalent 3R:4R (ref. 35). Cortical progenitor rosettes positive for the early forebrain marker Pax6 and the proliferation marker Ki67 were observed at day 20 of differentiation (Fig. 4e). At this time point, tau was observed in a subset of cells but did not colocalize with Ki67, suggesting that tau expression is restricted to postmitotic neurons. By day 100 of differentiation, the majority of cultured cells showed stereotypic neuronal morphology such as high levels of tau expression and extended neurites. To assess whether tau could be internalized, we transferred conditioned media from iPSCs to primary cultures of mouse wild-type neurons. After 6 d, hTau was observed in the neurites of the recipient cells with a similar distribution pattern to the tau generated by transgenic mouse neurons (Fig. 4f). This result is consistent with a recent finding showing that tau from both mouse and human brain extracts and from the ISF from the rTg4510 line are internalized by recipients²⁰.

Figure 6 Transfer of tau from cell to cell is enhanced by stimulating neuronal activity. (a) Images showing tau protein (green) from tau-expressing donor cells in recipient mCherry cells (red) (merged in yellow; arrows) seeded with clone 9 lysate. Data show cells stimulated without picrotoxin (C9 seeds + PBS) and with picrotoxin (C9 seeds + PTX). Scale bar, 50 μm . (b) Tau transfer, as determined by the number of mCherry cells containing tau, as a percentage of the total number of mCherry cells, was significantly higher in the stimulated group ($n = 5$) than in the unstimulated group ($n = 5$; $t_8 = -2.68$, $*P = 0.028$). Error bars represent \pm s.e.m.



Neuronal activity stimulates tau release and spread

Increased neuronal activity has been shown to stimulate tau release in wild-type and hTau-overexpressing transgenic mouse models *in vitro*²² and *in vivo*²³, but it is not known whether stimulation leads to release of tau from human neurons with physiological levels of tau. To examine this, we measured the amount of tau released into media from human iPSC neurons, from primary mouse neurons expressing endogenous tau and from neurons overexpressing mutant hTau (rTg4510 line), before and after treatment with picrotoxin, a noncompetitive channel blocker for the GABA receptor chloride channels³⁶ (Fig. 5a). In all three systems, stimulation with picrotoxin increased tau in the media by 150–210% compared to tau levels in the media before the addition of picrotoxin or compared to media from neurons treated with buffer alone, without causing cell death (Fig. 5b).

To examine whether increasing neuronal activity leads to enhanced tau release, we used an optogenetic approach in one of our culture models to directly stimulate neuronal action potentials³⁷. Cells expressing channelrhodopsin (ChR2) can be depolarized by exposure to blue light at a wavelength of 473 nm. Primary neurons from a wild-type mouse were transfected with fluorescently tagged hTau and ChR2 expressing viral vectors (Fig. 5c,d). Media were removed and analyzed for hTau levels before and after light stimulation. Whole-cell recording was performed simultaneously to confirm activation (Fig. 5e,f). After neurons were stimulated for 30 min (0.1 mW per mm^{-2} , 2-s intervals), tau in the media increased approximately 250% (Fig. 5g), reaching levels similar to the amount of tau released from neurons following picrotoxin treatment (Fig. 5a). Optogenetic stimulation did not result in cell death, as shown by patch

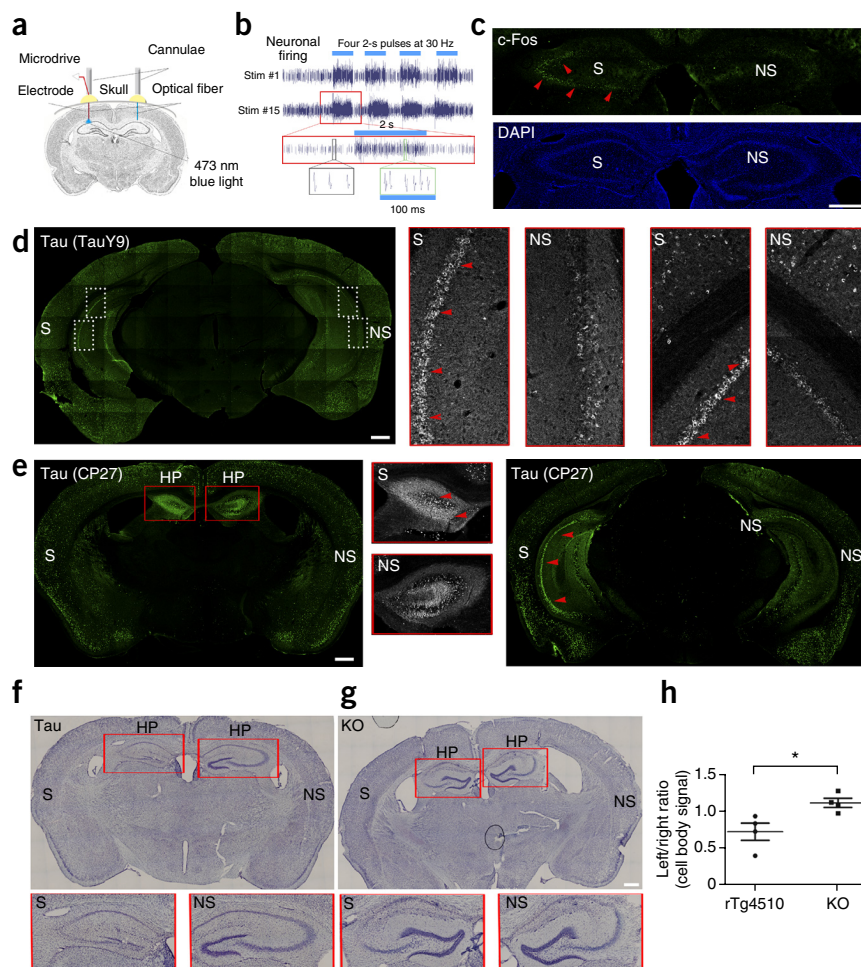


Figure 7 Optogenetically induced increased neuronal activity exacerbates tau pathology in the hippocampus. (a) *In vivo* optogenetic stimulation. Tau expressing mice (rTg4510) were injected with ChR2 expressing vector and implanted with optical fibers in both hemispheres; in some mice a recording electrode was also inserted in one or both hemispheres. (b) Extracellular recordings show that pulses of blue light (blue bars) increased the firing activity consistently. The same neurons could be recorded longitudinally (stimulations No. 1 and No. 15), demonstrating that chronic, repetitive stimulation did not impair cell viability. Red box, enlargement of stimulation No. 15; bottom row, example waveforms from stimulated (green inset) vs. unstimulated (black inset) neurons. (c) Representative image of c-Fos immunostaining. Top, increased c-Fos protein (green, arrowheads) in stimulated hemisphere. Bottom, DAPI stain of cell nuclei of the same tissue. Image is representative of two mice. Scale bar, 500 μm . (d) Brain tissues of stimulated mice labeled with anti-tau antibody (TauY9, green). Scale bar, 500 μm ; $n = 2$ mice; white boxes, enlargements of CA1 and CA3. (e) Posterior and anterior tissues labeled with anti-tau antibody (CP27, green) show more tau pathology (arrowheads, red) in the stimulated side. Red box, enlargements of anterior hippocampus. (f,g) Nissl stain of brain tissues of stimulated tau mouse and tau KO (tau KO-GFP line) shows reduced cell body staining, especially in the hippocampus. Scale bar, 500 μm ; $n = 4$ mice for each line. (h) Assessment of Nissl stain signal of hippocampal pyramidal cell layers shows a significant reduction in the stimulated hemisphere of the tau mice ($n = 4$) but not the tau KO mice ($n = 4$ mice, $z = 2.31$, $*P = 0.021$). S, stimulated hemisphere; NS, nonstimulated hemisphere. Error bars represent \pm s.e.m.

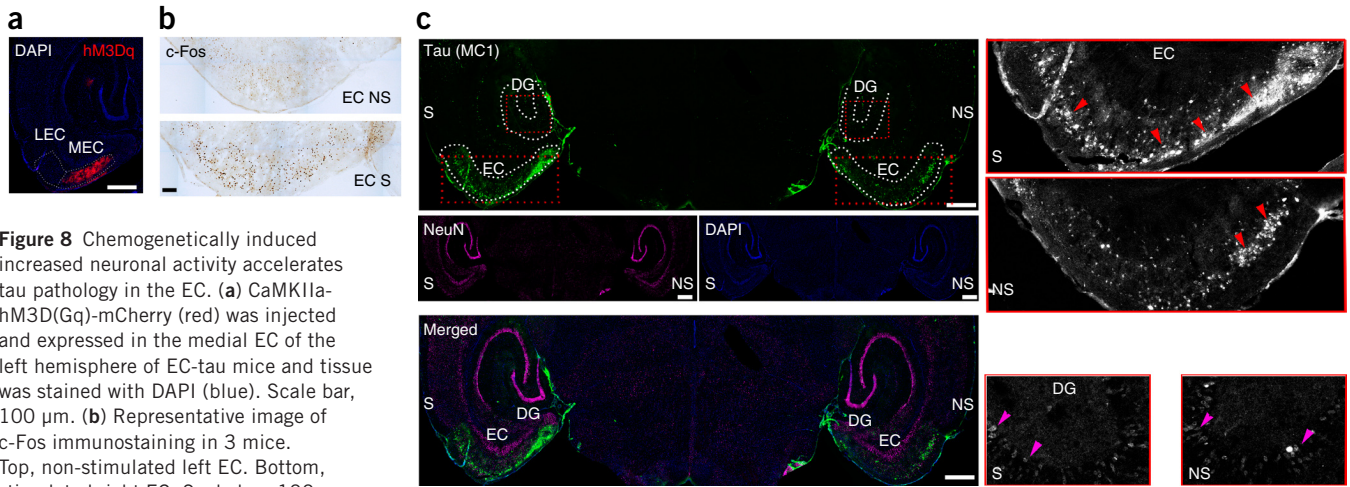


Figure 8 Chemogenetically induced increased neuronal activity accelerates tau pathology in the EC. (a) CaMKIIa-hM3D(Gq)-mCherry (red) was injected and expressed in the medial EC of the left hemisphere of EC-tau mice and tissue was stained with DAPI (blue). Scale bar, 100 μ m. (b) Representative image of c-Fos immunostaining in 3 mice. Top, non-stimulated left EC. Bottom, stimulated right EC. Scale bar, 100 μ m.

(c) Representative image of brain tissues of mice stimulated for 6 weeks labeled with an antibody against pathological hTau (MC1, green), anti-NeuN (magenta) and DAPI (blue) of stimulated and nonstimulated hemispheres. Red dotted boxes show insets: enlarged grayscale images (top right) of the EC (outlined in white dotted lines) and enlarged grayscale images (bottom right) of the dentate gyrus (DG; outlined in white dotted lines) represent green fluorescence staining (tau). Red arrowheads, somatodendritic tau in neurons of the EC; magenta arrowheads tau in granule cells of the DG; scale bars, 500 μ m; $n = 3$ mice; S, stimulated hemisphere; NS, nonstimulated hemisphere.

clamp recording of individual cells (Fig. 5e,f) and more globally by lactate dehydrogenase assessment (Fig. 5h). To test whether stimulating neuronal activity can enhance cell-to-cell transfer of tau, in addition to tau release, we added picrotoxin to cocultures of neurons that made hTau aggregates (RD-P301S-YFP with clone 9-seeded lysate) or mCherry (Fig. 6) and quantified the percent of mCherry cells containing YFP tau aggregates. After 2 weeks of coculture, neurons were fixed and examined using confocal microscopy (Fig. 6a). Quantification of immunofluorescence images demonstrated that stimulating neuronal activity increased the percentage of cells that had taken up tau from approximately 20% of mCherry cells to 45% of mCherry cells (Fig. 6b).

Enhanced neuronal activity accelerates tauopathy *in vivo*

Tau has been shown to accumulate in the ISF following administration of picrotoxin *in vivo*²³, but it is not known whether enhancing neuronal activity accelerates tauopathy. To address this question, we used two approaches to increase neuronal activity in two different tau mouse models. Using an optogenetic approach, ChR2 was expressed in neurons under the *Camk2a* (*CAMKIIA*) promoter³⁷ for 10 d and optical fibers were implanted in both left and right hippocampi of the rTg4510 line, but only the left hippocampus was stimulated with blue light (470 nm). Tau pathology in the left (stimulated) hemisphere was compared to the right (nonstimulated) hemisphere (Fig. 7a). *In vivo* recordings confirmed that blue light induced an increase in hippocampal activity (Fig. 7b). Neuronal firing in response to blue light was near-instantaneous, with minimal time lag (<10 ms), and the firing rate approximately doubled during stimulation. When the blue light was off, the firing rate returned to normal. The electroencephalogram (EEG) and spike firing pattern did not show any epileptic-like phenotype and seizures were not observed (data not shown). Recording from the right hemisphere showed that ChR2-controlled firing did not lead to firing in the nonstimulated hemisphere (data not shown). After 20 d of stimulation, mice were killed within 75 min of the last stimulation, and the brain tissue was processed for immunolabeling of the activity-induced immediate early gene *Fos* (*c-Fos*), which was readily observed in the stimulated hippocampus (Fig. 7c). When immunolabeled with anti-tau antibodies, we observed that the stimulated hippocampus had accumulated more hTau (labeled with TauY9 and

CP27 antibodies) in the cell bodies. This was particularly evident in the posterior and anterior planes, especially in CA1 and CA3 pyramidal cells (Fig. 7d,e), which was consistent with the placement of the optical fiber. Enhanced tau pathology was accompanied by hippocampal cell layer atrophy (Fig. 7e) that was more evident in brain tissues stained using Nissl (Fig. 7f,h). Optogenetic stimulation using the same parameters did not result in detectable atrophy in mice without tauopathy (a *MAPT*^{-/-} line; Fig. 7g,h), suggesting the stimulation itself was not causing the atrophy. To ensure that enhanced tauopathy was not due to enhanced expression of the transgene, we performed quantitative reverse transcriptase PCR (qRT-PCR) on both stimulated and nonstimulated hippocampal tissue from mice stimulated for 20 d. While there was variable hTau expression between mice, we did not detect differences in tau expression between hemispheres of rTg4510 mice (Supplementary Fig. 1).

To confirm our results using a different stimulation approach, in a different mouse line, we used the designer receptor exclusively activated by designer drug (DREADD)³⁸ chemogenetic approach to transiently stimulate neurons in the EC of the EC-tau mouse line². Clozapine-*n*-oxide (CNO)-responsive DREADD (CaMKIIa-hM3D(Gq)-mCherry) was expressed in the left EC and a receptor that is unresponsive to CNO (CaMKIIa-ChR2-mCherry) was expressed in the right EC as a control. The DREADD was expressed in the medial EC for at least 10 d before stimulation, and viral expression remained stable for at least 6 weeks (Fig. 8a). CNO administration enhanced neuronal activity in the medial EC approximately 20 min after injection without causing seizures, as shown by *in vivo* electrophysiology (data not shown), and enhanced c-Fos labeling in the stimulated EC compared to the nonstimulated EC (Fig. 8b). After 6 weeks of CNO administration, we observed increased accumulation of somatodendritic tau (antibody MC1) in neurons in the stimulated EC as compared to the nonstimulated EC of the same mouse (Fig. 8c). Stimulation for 2 weeks also produced enhanced tauopathy, but to a lesser degree (Supplementary Fig. 2a). Images taken using higher laser power demonstrated that the increase in somatodendritic tau was most evident in the EC region where DREADD virus was expressed, whereas tau pathology in other regions (for example, the granule cells of the dentate

gyrus) did not show any obvious enhancement (Fig. 8c). A similar enhancement of tau pathology was observed using a second human-specific tau antibody, CP27 (Supplementary Fig. 3b). Nonspecific staining was not observed when the secondary antibody was used in the absence of the primary antibody (data not shown).

DISCUSSION

Using a variety of *in vitro* cell models, we have shown that (1) neuron-derived full-length tau can transfer to recipients and aggregated tau can be induced by seeding transfers efficiently, (2) neuron-derived tau can not only be internalized by recipient neurons but can also undergo transcellular propagation to distant cells, and (3) neuron-derived tau (including tau from human iPSCs) can transfer to recipients via the extracellular space. Several studies have shown internalization of exogenously added tau^{8,9,12,39,40} into recipient cells, while more recent studies show that endogenously generated tau can also be internalized, including tau that was released into the extracellular space either in conditioned media from mutant-tau-expressing human neuroblastoma-derived SH-SY5Y cells⁴¹ or the ISF from rTg4510 mice²³. In our study we found that nonmutant tau from wild-type mice and from nonmutant human iPSCs can also be released and internalized. Tau in these cells does not form overt, morphologically distinct aggregates even when cultured for long periods of time (>20 d; data not shown), suggesting that the majority of tau released from these neurons is likely to be soluble, which is consistent with a study showing that soluble tau is released into the medium of cells²², the ISF of transgenic and wild-type mice^{18,23} and the ISF of an anti-aggregating mouse model⁴². Whether the soluble tau from wild-type neurons or iPSCs is monomeric or oligomeric is unknown. Exogenously added monomeric tau can be internalized⁴¹, but in our experience⁹ it does not accumulate to any degree. It is possible, especially for neurons from the rTg4510 line, that small, early-stage misfolded tau oligomers that are not readily discernible by morphology, nor by dyes such as X-34 that recognize more aggregated beta-sheet structures, have formed in the cultures and that these oligomers are released into the media and taken up by recipient neurons. What is clear from our seeding experiments, however, is that higher order aggregated forms of tau can accumulate in recipients more readily. A recent study²³ examining the uptake of tau from brain extract shows that a low-abundance, higher molecular weight, phosphorylated form of tau is internalized and propagates. The same study shows that both high and low molecular weight tau is present in the ISF from rTg4510 mice, and while tau in the ISF is internalized by recipients, it is not known whether it is the same type of tau that is internalized from the lysate. In our experience, tau released from cells making aggregates promotes propagation much more robustly than tau from neurons making soluble tau. Taking advantage of this observation, we found that tau aggregates generated in one population of neurons can induce tau misfolding (X-34-positive aggregates) in fluidically isolated second and third populations of neurons cultured in microfluidic chambers.

The fact that tau can be transferred between cells via the medium suggests that structures such as tunneling nanotubes are not required, at least not for *in vitro* transfer (*in vivo* transfer mechanisms are not known). We do not yet know whether tau in the medium is vesicle-bound or free. Exogenously added free (recombinant) tau^{12,39,43}, including oligomers⁹, has been shown to be internalized by bulk endocytosis, and uptake can be mediated by binding to heparan sulfate proteoglycans⁴³. Exogenously added tau in cell or brain extract can also be internalized by recipient cells^{8,44,45}, but it is not known whether it is free or vesicle-bound in these preparations. A small proportion of

tau released from cells (for example, into the ISF of rodents overexpressing wild-type tau¹⁷) has been identified in vesicles (ectosomes and to a lesser extent exosomes). Tau has only been found in ectosomes and not exosomes when it is expressed at physiological levels¹⁷. Using wild-type neurons and iPSCs, we have shown that tau release and internalization can occur without the overexpression of tau. How internalized tau accesses endogenous tau to enable templating is unknown, but the creation of more physiologically relevant models of tau release, internalization and propagation such as those described here will allow us to address these questions better. Taken together, our data show that endogenously produced tau aggregates are released and can induce subsequent misfolding and seed formation in downstream neurons, resulting in cell-to-cell propagation that could explain the widespread distribution of tau pathology in AD.

One observation from transgenic mice overexpressing the amyloid precursor protein is that elevated amyloid beta is associated with hyperexcitability at the cellular level^{24–28}. The observation that cellular hyperexcitability can stimulate the release of tau *in vitro*²² and *in vivo*²³ suggests that, in humans, amyloid beta-induced hyperexcitability in regions of the brain that are vulnerable to early tauopathy, such as the hippocampal formation, could lead to enhanced release of pathogenic tau and accelerated propagation of tauopathy through circuits. In support of this, we have shown that optogenetically stimulated rTg4510 tau mice undergo robust worsening of pathology (accumulation of cell body tau) in the stimulated hippocampus. The worsened pathology appears to be neurotoxic, as it correlated with exacerbated hippocampal cell layer atrophy. The EC-tau mouse model, when stimulated chemogenetically, demonstrated worsening tauopathy in the stimulated EC. Additional pathology in cell populations that are synaptically connected with the EC, such as the dentate gyrus granule cell layer, was not obvious. However, in the EC-tau line, the accumulation of tau in the granule cell layer is a slow process that takes more than 18 months to become apparent². In our experiments, the EC was stimulated for a maximum of 6 weeks, starting at an age when pathology was mild. More time may be needed to effectively induce tau propagation into the granule cells of the dentate gyrus, or the mice may need to be at a more advanced stage of pathology when first stimulated for it to become apparent within the relatively short timeframe. In general, these data have several implications. First, they may have relevance for AD, where therapeutic approaches to dampen excitability^{46–48} may retard the spread of tau pathology, which, if performed during the earliest Braak stages, could prevent the onset of cognitive decline that usually starts during the later Braak stages. Second, these results may explain the observation of tauopathy associated with epileptic seizures, although the link between brain injury and tauopathy obscures the relationship⁴⁹. Lastly, there may be negative implications for stimulation therapies such as deep brain stimulation or transcranial magnetic stimulation that are currently in clinical trials for AD.

METHODS

Methods and any associated references are available in the [online version of the paper](#).

Note: Any Supplementary Information and Source Data files are available in the online version of the paper.

ACKNOWLEDGMENTS

We thank C. Acker for help with Sandwich ELISA and P. Davies (Litwin Zucker Center for Alzheimer's Research, Feinstein Institute, New York, USA) for providing tau antibodies. We thank K. Jansen-West, E. Perkerson and L. Petrucci (Mayo Clinic Jacksonville) for providing additional tau viruses and

D. Sulzer for discussions regarding cell electrophysiology. We also thank L. Liu for assistance with mouse tissue collection, C. Profaci for assistance with optogenetic experiments and L. Shi for administrative assistance. This work was supported by a BrightFocus Foundation fellowship to J.W., NIH/NINDS grants NS081555 and NS074874 to K.E.D., Cure Alzheimer's Fund to K.E.D., the Parkinson's Disease Foundation to D.S. and NIH/NIA grant AG050425 to S.A.H. and K.E.D. A.M. is supported by funds from NIH/NIA AA19801. S.W. is supported by the NIHR Queen Square Dementia Biomedical Research Unit.

AUTHOR CONTRIBUTIONS

J.W.W. and K.E.D. designed the experiments. J.W.W., S.A.H., I.M.B., A.M. and S.W. conducted the experiments and data analyses. J.W.W., C.L.C. and K.E.D. wrote the manuscript. M.H., E.N., S.E. and Y.H.F. provided technical assistance. S.A.H., I.M.B., G.A.R. and Y.H.F. performed mouse surgery, *in vivo* recordings, *in vivo* stimulations and immunohistochemistry. A.M. performed *in vitro* patch-clamp experiments, and providing the LED microscope, optimization of *in vitro* optogenetic stimulation. K.R. and C.L.C. performed the qRT-PCR experiment and, together with C.C., performed AAV P301L-GFP, GFP and WT-GFP virus cloning, packaging and titration. C.L.C. performed statistical analyses. D.W.S. and M.I.D. provided cell lysates containing tau seeds and repeat-domain PSY, YFP and mCherry viruses. I.M.B. performed Nissl and immunofluorescence analysis. S.W. performed iPSC differentiation and data analysis and provided conditioned media. R.A.C.M.B. performed immunoprecipitation of tau from conditioned media and cell lysates.

COMPETING FINANCIAL INTERESTS

The authors declare no competing financial interests.

Reprints and permissions information is available online at <http://www.nature.com/reprints/index.html>.

- Braak, H. & Braak, E. Neuropathological staging of Alzheimer-related changes. *Acta Neuropathol.* **82**, 239–259 (1991).
- Liu, L. *et al.* Trans-synaptic spread of tau pathology *in vivo*. *PLoS One* **7**, e31302 (2012).
- de Calignon, A. *et al.* Propagation of tau pathology in a model of early Alzheimer's disease. *Neuron* **73**, 685–697 (2012).
- Harris, J.A. *et al.* Human P301L-mutant tau expression in mouse entorhinal-hippocampal network causes tau aggregation and presynaptic pathology but no cognitive deficits. *PLoS One* **7**, e45881 (2012).
- Clavaguera, F. *et al.* Brain homogenates from human tauopathies induce tau inclusions in mouse brain. *Proc. Natl. Acad. Sci. USA* **110**, 9535–9540 (2013).
- Clavaguera, F. *et al.* Transmission and spreading of tauopathy in transgenic mouse brain. *Nat. Cell Biol.* **11**, 909–913 (2009).
- Iba, M. *et al.* Synthetic tau fibrils mediate transmission of neurofibrillary tangles in a transgenic mouse model of Alzheimer's-like tauopathy. *J. Neurosci.* **33**, 1024–1037 (2013).
- Sanders, D.W. *et al.* Distinct tau prion strains propagate in cells and mice and define different tauopathies. *Neuron* **82**, 1271–1288 (2014).
- Wu, J.W. *et al.* Small misfolded Tau species are internalized via bulk endocytosis and anterogradely and retrogradely transported in neurons. *J. Biol. Chem.* **288**, 1856–1870 (2013).
- Caillierez, R. *et al.* Lentiviral delivery of the human wild-type tau protein mediates a slow and progressive neurodegenerative tau pathology in the rat brain. *Mol. Ther.* **21**, 1358–1368 (2013).
- Osinde, M., Clavaguera, F., May-Nass, R., Tolnay, M. & Dev, K.K. Lentivirus Tau (P301S) expression in adult amyloid precursor protein (APP)-transgenic mice leads to tangle formation. *Neuropathol. Appl. Neurobiol.* **34**, 523–531 (2008).
- Kfoury, N., Holmes, B.B., Jiang, H., Holtzman, D.M. & Diamond, M.I. Trans-cellular propagation of Tau aggregation by fibrillar species. *J. Biol. Chem.* **287**, 19440–19451 (2012).
- Gousset, K. *et al.* Prions hijack tunnelling nanotubes for intercellular spread. *Nat. Cell Biol.* **11**, 328–336 (2009).
- Saman, S. *et al.* Exosome-associated tau is secreted in tauopathy models and is selectively phosphorylated in cerebrospinal fluid in early Alzheimer disease. *J. Biol. Chem.* **287**, 3842–3849 (2012).
- Asai, H. *et al.* Depletion of microglia and inhibition of exosome synthesis halt tau propagation. *Nat. Neurosci.* **18**, 1584–1593 (2015).
- Simón, D. *et al.* Tau overexpression results in its secretion via membrane vesicles. *Neurodegener. Dis.* **10**, 73–75 (2012).
- Dujardin, S. *et al.* Ectosomes: a new mechanism for non-exosomal secretion of tau protein. *PLoS One* **9**, e100760 (2014).
- Yamada, K. *et al.* *In vivo* microdialysis reveals age-dependent decrease of brain interstitial fluid tau levels in P301S human tau transgenic mice. *J. Neurosci.* **31**, 13110–13117 (2011).
- Barten, D.M. *et al.* Tau transgenic mice as models for cerebrospinal fluid tau biomarkers. *J. Alzheimers Dis.* **24** (suppl.) 2: 127–141 (2011).
- Takeda, S. *et al.* Neuronal uptake and propagation of a rare phosphorylated high-molecular-weight tau derived from Alzheimer's disease brain. *Nat. Commun.* **6**, 8490 (2015).
- Kurz, A. *et al.* Tau protein in cerebrospinal fluid is significantly increased at the earliest clinical stage of Alzheimer disease. *Alzheimer Dis. Assoc. Disord.* **12**, 372–377 (1998).
- Pooler, A.M., Phillips, E.C., Lau, D.H., Noble, W. & Hanger, D.P. Physiological release of endogenous tau is stimulated by neuronal activity. *EMBO Rep.* **14**, 389–394 (2013).
- Yamada, K. *et al.* Neuronal activity regulates extracellular tau *in vivo*. *J. Exp. Med.* **211**, 387–393 (2014).
- Busche, M.A. *et al.* Clusters of hyperactive neurons near amyloid plaques in a mouse model of Alzheimer's disease. *Science* **321**, 1686–1689 (2008).
- Busche, M.A. *et al.* Critical role of soluble amyloid- β for early hippocampal hyperactivity in a mouse model of Alzheimer's disease. *Proc. Natl. Acad. Sci. USA* **109**, 8740–8745 (2012).
- Šišková, Z. *et al.* Dendritic structural degeneration is functionally linked to cellular hyperexcitability in a mouse model of Alzheimer's disease. *Neuron* **84**, 1023–1033 (2014).
- Minkeviciene, R. *et al.* Amyloid beta-induced neuronal hyperexcitability triggers progressive epilepsy. *J. Neurosci.* **29**, 3453–3462 (2009).
- Hall, A.M. *et al.* Tau-dependent Kv4.2 depletion and dendritic hyperexcitability in a mouse model of Alzheimer's disease. *J. Neurosci.* **35**, 6221–6230 (2015).
- Santacruz, K. *et al.* Tau suppression in a neurodegenerative mouse model improves memory function. *Science* **309**, 476–481 (2005).
- Tucker, K.L., Meyer, M. & Barde, Y.A. Neurotrophins are required for nerve growth during development. *Nat. Neurosci.* **4**, 29–37 (2001).
- Taylor, A.M. *et al.* A microfluidic culture platform for CNS axonal injury, regeneration and transport. *Nat. Methods* **2**, 599–605 (2005).
- Styren, S.D., Hamilton, R.L., Styren, G.C. & Klunk, W.E. X-34, a fluorescent derivative of Congo red: a novel histochemical stain for Alzheimer's disease pathology. *J. Histochem. Cytochem.* **48**, 1223–1232 (2000).
- Shi, Y., Kirwan, P. & Livesey, F.J. Directed differentiation of human pluripotent stem cells to cerebral cortex neurons and neural networks. *Nat. Protoc.* **7**, 1836–1846 (2012).
- Shi, Y., Kirwan, P., Smith, J., Robinson, H.P. & Livesey, F.J. Human cerebral cortex development from pluripotent stem cells to functional excitatory synapses. *Nat. Neurosci.* **15**, 477–486 (2012).
- Sposito, T. *et al.* Developmental regulation of tau splicing is disrupted in stem cell-derived neurons from frontotemporal dementia patients with the 10 + 16 splice-site mutation in MAPT. *Hum. Mol. Genet.* **24**, 5260–5269 (2015).
- Yoon, K.W., Covey, D.F. & Rothman, S.M. Multiple mechanisms of picrotoxin block of GABA-induced currents in rat hippocampal neurons. *J. Physiol. (Lond.)* **464**, 423–439 (1993).
- Boyden, E.S., Zhang, F., Bamberg, E., Nagel, G. & Deisseroth, K. Millisecond-timescale, genetically targeted optical control of neural activity. *Nat. Neurosci.* **8**, 1263–1268 (2005).
- Zhu, H. & Roth, B.L. DREADD: a chemogenetic GPCR signaling platform. *Int. J. Neuropsychopharmacol.* **18**, pyu007 (2015).
- Frost, B., Jacks, R.L. & Diamond, M.I. Propagation of tau misfolding from the outside to the inside of a cell. *J. Biol. Chem.* **284**, 12845–12852 (2009).
- Guo, J.L. & Lee, V.M. Seeding of normal Tau by pathological Tau conformers drives pathogenesis of Alzheimer-like tangles. *J. Biol. Chem.* **286**, 15317–15331 (2011).
- Michel, C.H. *et al.* Extracellular monomeric tau protein is sufficient to initiate the spread of tau protein pathology. *J. Biol. Chem.* **289**, 956–967 (2014).
- Yamada, K. *et al.* Analysis of *in vivo* turnover of tau in a mouse model of tauopathy. *Mol. Neurodegener.* **10**, 55 (2015).
- Holmes, B.B. *et al.* Heparan sulfate proteoglycans mediate internalization and propagation of specific proteopathic seeds. *Proc. Natl. Acad. Sci. USA* **110**, E3138–E3147 (2013).
- Mirbaha, H., Holmes, B.B., Sanders, D.W., Bieschke, J. & Diamond, M.I. Tau trimers are the minimal propagation unit spontaneously internalized to seed intracellular aggregation. *J. Biol. Chem.* **290**, 14893–14903 (2015).
- Santa-Maria, I. *et al.* Paired helical filaments from Alzheimer disease brain induce intracellular accumulation of Tau protein in aggregates. *J. Biol. Chem.* **287**, 20522–20533 (2012).
- Bomben, V. *et al.* Bexarotene reduces network excitability in models of Alzheimer's disease and epilepsy. *Neurobiol. Aging* **35**, 2091–2095 (2014).
- Sanchez, P.E. *et al.* Levetiracetam suppresses neuronal network dysfunction and reverses synaptic and cognitive deficits in an Alzheimer's disease model. *Proc. Natl. Acad. Sci. USA* **109**, E2895–E2903 (2012).
- Busche, M.A. *et al.* Rescue of long-range circuit dysfunction in Alzheimer's disease models. *Nat. Neurosci.* **18**, 1623–1630 (2015).
- Thom, M. *et al.* Neurofibrillary tangle pathology and Braak staging in chronic epilepsy in relation to traumatic brain injury and hippocampal sclerosis: a post-mortem study. *Brain* **134**, 2969–2981 (2011).

ONLINE METHODS

Transgenic mice. Protocols and procedures were approved by the Committee on the Ethics of Animal Experiments of Columbia University and according to Guide for the Care and Use of Laboratory Animals of the National Institutes of Health. Mouse models used in this study included: rTg4510 (CAMKII: hTau-P301L; embryonic day 15–16 for culture and 2–4 months for *in vivo* studies; parental lines were a gift of K. Hsiao)²², *MAPT*^{-/-}:GFP (tau knockout-GFP) (embryonic day 15–16; parental line was a gift of K. Tucker)³⁰, tau knockout (Jackson Labs), and EC-tau (neurosin-tTA, hTau-P301L line r4510; 12–14 months; parental lines were a gift of M. Mayford and K. Hsiao)². Both male and female mice were used for each *in vivo* experiment. Strains of mice were C129/FVB F1 (rTg4510) and C57Blk6 (hTau and tau knockout).

Neuronal cultures. Primary neuronal cultures were prepared and maintained as previously described⁹. For cocultures, hippocampal and cortical neurons were isolated from male and female rTg4510 and tau knockout-GFP mouse lines, plated into separate reservoirs of the MFs or together at 1:1 ratios on coverslips. For cocultures of transduced neurons, male and female wild-type rat primary neurons were plated in MFs and then transduced at 3–5 DIV with either mCherry (1:1,000) or tau-GFP (hTau-P301L-GFP or GFP alone, 2×10^9 particles), or RD P301S YFP (1:10) vectors. Amounts of tau protein generated in cultured neurons were as follows: P301L GFP transduced neurons: $9.28 \pm 0.675 \mu\text{g mg}$ (tau per total protein) ($n = 3$ cultures); rTg4510 neurons: $7.84 \pm 1.97 \mu\text{g mg}$ (tau per total protein) ($n = 12$ cultures); WT neurons: $2.81 \pm 1.14 \mu\text{g mg}$ (tau per total protein) ($n = 12$ cultures); iPSC neurons: $6.05 \pm 1.07 \mu\text{g mg}$ (tau per total protein) ($n = 12$ cultures). For seeding experiment, 2.5 μg of clone 1 or clone 9 lysates prepared as previously described were added to neurons that were transduced with RD P301S YFP at 6–8 DIV, and cultured for an additional 9–10 d.

Neural induction. iPSCs were differentiated into cortical neurons. Briefly, iPSCs were converted to neural epithelium using the dual SMAD inhibitors dorsomorphin and SB431452, followed by an extended period of *in vitro* neurogenesis to generate cortical glutamatergic neurons. Neurons were maintained in a 1:1 mixture of N-2 medium and B-27 medium³³, changed every 48 h. Neuron-conditioned media were prepared by collecting media after 48 h, centrifuging at 3,000g for 10 min to remove cell debris and stored at -80°C .

Immunoprecipitation. Neurons were transduced with either tau-GFP or GFP (75,000 neurons / well, tau-P301L-GFP, 2×10^9 particles; GFP, 2×10^9 particles). Media from wild-type (wt), GFP-expressing or tau-expressing cells were collected every 3–4 d from mature neurons (tau or tau-GFP, 14–21 DIV) and centrifuged at 3,000g for 10 min at 4°C to remove cell debris. At the end of collection, cells were harvested in RIPA buffer with protease and phosphatase inhibitors ($1 \mu\text{g ml}^{-1}$, Sigma). For immunoprecipitation of tau, magnetic anti-mouse protein A Dynabeads (ThermoFisher Scientific, 11201D) were incubated with hTau-specific antibody (CP27, mouse) at a 2:1 ratio overnight, washed 3 times with 0.1% BSA in PBS and incubated with either conditioned media or cell lysates for 2 h at 4°C . Beads were isolated using a magnetic stir bar and resuspended in loading buffer for western blot analysis.

Immunoblot. Immunoprecipitated samples were prepared and analyzed by immunoblot as previously described, except that membranes were probed with rabbit anti-tau (TauC, 1:2,000, Dako, A0024) and anti-actin (1:500, Sigma, A5060) antibodies. For human iPSC western blot, cells were harvested in buffer containing protease and phosphatase inhibitors (Roche). Equal amounts of protein were dephosphorylated using lambda protein phosphatase (NEB) before separation on 4–12% NuPage gels (Invitrogen). Recombinant tau ladder (Sigma) was used to identify specific tau isoforms. Proteins were transferred to nitrocellulose membranes and blocked with 3% milk in PBS before incubation with anti-tau antibody (total tau, DAKO, A0024) O/N at 4°C . Membranes were incubated with IRDye 800–conjugated goat anti-rabbit (Rockland Inc, 611-145-122) and proteins were visualized using the Odyssey Infrared imaging system (LiCor Biosciences). For western blot analysis of human iPSC neurons, cells were lysed in 10 mM Tris, pH 7.4, 100 mM NaCl, 1 mM EDTA, 1 mM EGTA, 1% Triton X-100, 10% glycerol, 0.1% SDS, 0.5% deoxycholate, plus protease and phosphatase inhibitors (Roche) for 1 h at 4°C . Proteins were separated on SDS-PAGE BisTris

gels (NuPAGE Novex, 4–12%, Invitrogen) and subsequently transferred onto nitrocellulose membranes. Membranes were blocked in phosphate buffered saline containing 3% milk (PBS-M) for 1 h at room temperature. Membranes were incubated in primary antibody (DAKO polyclonal antibody to total tau, dilution 1:10,000, A0024) in PBS-M overnight at 4°C . Blots were developed with IRDye 800–conjugated goat anti-rabbit (Rockland Inc, 611-145-122) or IRDye 680–conjugated goat anti-mouse (Molecular Probes, A21058) and visualized using an Odyssey Infrared Imaging System (Li-Cor Biosciences). For analysis of tau isoforms, samples were dephosphorylated before electrophoresis using lambda protein phosphatase and separated by SDS-PAGE alongside a recombinant tau ladder (Sigma).

Tau ELISA. Mature tau knockout-GFP neurons were exposed to tau-conditioned media for 6 h, 12 h, 1 d and 6 d, washed three times with warmed PBS, trypsinized for 2 min, collected and homogenized in buffer supplemented with protease and phosphatase inhibitors at 4°C . Protein concentration was determined by BCA Assay (Pierce) and normalized with $1 \times$ PBS. Sandwich ELISA was performed as previously described using tau monoclonal antibodies DA31 and DA9-HRP (gifts from Dr. Peter Davies)⁵⁰.

Viral vectors. Tau RD-P301S YFP (aa 244–372 of the 441 amino acids in full-length tau; mutations P301S; “PS”), YFP and mCherry viruses were prepared by transient cotransfection of HEK293T cells with indicated vectors using calcium phosphate method. Media containing virus were collected 48 h after transfection and purified using Lenti-X-Concentrator according to manufacturer’s protocol (Clontech). Wild-type and P301L 4R2N tau constructs were cloned into an eGFP-AAV1 vector (chicken β -actin promoter), and all sequences were verified. AAV was subsequently produced and the genomic titer of each virus was determined by quantitative PCR.

RNA extraction and quantitative RT-PCR. RNA was extracted from 5–10 mg of hippocampal tissue from three 7-month-old mice (rTg4510 line, two male and one female) that were optogenetically stimulated for 20 d as described above, plus three 2- to 3-month-old animals that had been stimulated for 5 d, using a standard Trizol procedure. SuperScript[®] III RT enzyme and SuperMix (Invitrogen[™], Carlsbad, CA) containing 2.5 μM oligo(dT)₂₀, 2.5 $\text{ng } \mu\text{L}^{-1}$, random hexamers, 0.1 mM MgCl₂ and dNTPs, was used for first strand cDNA synthesis in a 20 μL reaction volume. Gene expression was assessed using TaqMan[®] probes (ThermoFisher Scientific, Waltham, MA) for the human *MAPT* transgene (Hs00902194_m1), mouse *NeuN (Rbfox3)* (Mm01248771_m1) and the mouse hypoxanthine guanine phosphoribosyl transferase gene (*Hprt*) (Mm03024075). PCRs were performed by monitoring in real time the increase in fluorescence of the FAM and VIC fluorophores, using an iQ5 detector system (Bio-Rad, Hercules, CA). All samples were run in triplicate 20 μL duplexed PCR reactions using 1 μL each of FAM and VIC labeled TaqMan[®] probes, 10 μL of TaqMan[®] Gene Expression Master Mix (Applied Biosystems, Foster City, CA), and 8 μL of diluted cDNA (1:40), using amplification conditions as follows: 50°C for 2 min, followed by 95°C for 10 min and 40 cycles of denaturation at 95°C (15 s), and priming, extension and data capture at 60°C (60 s). A standard curve was generated for each gene using dilutions of cDNA pooled from each sample. Relative expression changes were calculated using the $2^{-\Delta\Delta\text{CT}}$ method, defined as the ΔCT of the sample normalized to the housekeeping gene *Hprt*, minus the ΔCT of the normalized reference sample from the standard curve.

In vitro stimulation and cell viability assessment. To induce activity, neurons at 12–14 DIV were treated with picrotoxin (100 μM) for 30 min without changing the medium. For optogenetic stimulation, neurons were transduced with tau (tau-P301L-GFP, 2×10^9 particles) and Chr2 (AAV9.CaMKIIa.hChr2(H134R)-mCherry.WPRE.hGH; Penn Vector Core, 3.98×10^{11} particles) at 3–5 DIV. After 9–12 DIV, control wild-type or transduced neuronal cultures were placed on an upright microscope (Olympus) and stimulated with blue light (470 nm) at 0.1 mW mm^{-2} (40 mA) for 30 min at 2-s intervals. The emission power was measured using a power meter (ThorLabs) placed directly below and at the same distance from the objective lens as the cultures. The chamber temperature was maintained at $32^\circ\text{C} \pm 2^\circ\text{C}$. Media were collected before and after stimulation, centrifuged to remove cell debris, and analyzed by Sandwich ELISA using tau

monoclonal antibodies DA31 and DA9-HRP⁵⁰ in duplicates. Cell death was quantified by measuring LDH release in the same neuronal populations before and after treatments, according to the manufacturer's protocol (Promega).

Whole-cell patch clamp recordings. Mature neuronal cultures (DIV 12–14) were placed on the recording chamber (Warner Instruments) of an upright microscope equipped with 10× and 40× oil-immersion objectives (Olympus). Control and transduced neurons were identified by DIC optics and fluorescence, respectively. Cells were perfused with artificial cerebrospinal fluid (ACSF) containing (in mM) 119 NaCl, 26.2 NaHCO₃, 10 glucose, 2.4 CaCl₂, 3.6 KCl, 1.2 MgCl₂, and 1.0 NaH₂PO₄ at < 0.5 ml min⁻¹ flow rate. The chamber temperature was maintained at 32 °C ± 2 °C. Whole-cell patch clamp recordings were made with pulled borosilicate glass pipettes (G150F-4, Warner Instruments, tip resistance 2–4 MΩ) filled with intracellular solution containing (in mM): 115 potassium gluconate, 20 KCl, 10 HEPES, 2 MgCl₂, 2 ATP-Mg, 2 ATP-Na₂ and 0.3 GTP-Na (pH = 7.25, ~300 mOsm). Whole cell current clamp recordings were performed with an Axopatch 200B amplifier (Molecular Devices) and digitized at 10 kHz with a Digidata 1332 (Molecular Devices). Data were acquired using Clampex 8.2 software (Molecular Devices) for subsequent analysis. Blue light (470 nm) or control red light (545 ± 30 nm) was delivered by an LED controller (Thorlabs, 40 mA) and triggered with a Master-8 pulse generator (A.M.P.I. Labs). Synaptic inputs were blocked with picrotoxin (50 μM) and NBQX (20 μM) (Sigma-Aldrich). The input resistance and the baseline resting membrane potential were monitored throughout the recording. Current-voltage relationships were measured by injecting step current from -300 to +150 pA at +50 pA increments. Data were analyzed in Clampfit (Molecular Devices).

Surgery. Surgical procedures were performed following NIH guidelines in accordance with IACUC protocols. Mice were anesthetized with ketamine/xylazine (100 mg ml⁻¹, 15 mg ml⁻¹, respectively). AAV5 CamKII.hM3Dq-mCherry (1.7 × 10¹² particles; Gene Therapy Vector Core at the University of North Carolina, Chapel Hill) and AAV9/CamKIIa.hChR2-mCherry (2 × 10¹² particles; Penn Vector, AV-1-26975) virus were injected into the MEC (0.2–0.3 mm in front of the transverse sinus (AP), 3.0–3.1 mm (ML), and 1.5 mm below the dura (DV)) of the left or right hemisphere of rTg4510mice, respectively. For *in vivo* optogenetic experiments, AAV9/CamKIIa.hChR2-mCherry (2 × 10¹² particles) virus was injected into the hippocampus (1.5 mm (DV), 1.8 mm (ML), 1.8 mm (AP)) of both the left and right hemispheres of rTg4510mice. A 20 mm cannula was implanted slightly above the injection site (~1.2 mm) in both brain hemispheres. For one mouse, a microdrive was implanted in the left hemisphere (~1.2 mm depth) to record neuronal activity. Dental cement was used to secure the cannulae and microdrive.

***In vivo* chemogenetic stimulation and electrophysiology.** Ten days following viral DREADD transduction, CNO was given to mice systemically via intraperitoneal injections at 5 mg kg⁻¹, 2 times per day (6–7 h between injections), 5 d per week for either 2 or 6 weeks. Total stimulation was either 20 or 60 times. Injections were alternated between left and right sides of the mouse to minimize scarring. CNO (C-929) was generously provided by the National Institutes of Mental Health Chemical Synthesis and Drug Supply Program. Both male and female mice were used.

***In vivo* optogenetic stimulation and electrophysiology.** Ten days following ChR2 viral transduction, the left hemisphere of mice was optically stimulated with four pulses of LED light (470 nm) (Thorlabs) at 30 Hz frequency, 3 times with -a 1-min interval. Mice were stimulated 3 times per d, 5 times per week for 4 weeks (60 stimulations total). The right hemisphere was not stimulated to provide a within-animal control. To record neuronal activity, the mouse implanted with electrodes was plugged into the electrophysiology setup (Axona) during stimulation and neuronal activity was recorded. Individual neurons from the recording data were separated using the spike sorting software Tint (Axona). Neurons were identified based on spike-firing rate, amplitude, waveform and their refractory periods. sigTOOL (a Matlab-based signal analysis tool) was used to visualize changes in neuronal firing during optical stimulation. Both male and female mice were used.

Immunofluorescence, Nissl and DAB staining. Mouse brains were collected as described previously. Free-floating sections in either coronal or horizontal plane

(35 μm) were used for immunofluorescence. Human iPSC neurons were grown in 8-well chamber slides (Ibidi) and primary neurons were grown as previously described. Neurons and free-floating tissues were immunolabeled and mounted as previously described with the following antibodies: mouse anti-tau (CP27, 1:1,000 MC1, 1:2,000; gifts of P. Davies)², rabbit anti-GFP (1:500, Abcam, Ab6556), total tau (TauC, DAKO, 1:5,000, A0024), 3R tau (RD3, Millipore, 1:1,000), Pax6 (Covance, 1:300, PRB-278P) and Ki67 (BD Biosciences, 1:500, 550609). Fluorescently conjugated secondary antisera mixtures containing Alexa 488 IgG, Alexa 594 IgG or Alexa 647 IgG (ThermoFisher Scientific, A-11001, A-11037, A-21245 and A0-21235) were used. Antigen retrieval was performed on tissues by heating in sodium citrate for 5 min at 95 °C. Tissues were treated with sudan black (0.1% in PBS) for 10–15 min to eliminate autofluorescence from lipofuscin. For Nissl staining, sections were stained with 0.1% cresyl violet in 70% EtOH for 10 min at RT, rinsed with distilled H₂O, washed three times with PBS and mounted with Prolong anti-fade medium (Invitrogen). DAB staining on tissues was performed as previously described². Briefly, tissues were treated with 5% H₂O₂ in PBS for 10 min to quench endogenous peroxidase activity, blocked in PBS containing 5% horse serum and 0.3% Triton, and incubated at 4 °C overnight as previously described² with the following antibodies: c-Fos (1:200, Santa Cruz, G3115), AT8 (S202/205, 1:1,000, ThermoFisher, MN1020), MC1 (conformationally abnormal hTau, 1:1,000). After three washes with PBS-T, tissues were developed using Super Picture HRP (Invitrogen) for 15 min at room temperature on a rotator and detection of the chromagen with DAB (Sigma-Aldrich) was done according to the manufacturer's manual. In the case of c-Fos staining, mice were killed 75 min after their last CNO injection. An ABC kit (Vectastain, Vector Labs) was used to develop the tissues according to the manufacturer's manual. The sections were mounted and were visualized by light microscopy.

Confocal and light microscopy. Immunolabeled neurons and tissues were examined with a Zeiss LSM710 confocal microscope at 10× dry and 63× oil immersion objectives as previously described. Sequential tile scans were performed to capture wide-field images of microfluidics (at 1,024 × 1,024 resolution) and tissues (512 × 512). Sequential scans were performed to capture images of cells grown on coverslips (1,024 × 1,024). All images from the same experiment were taken at the same laser intensity and detector gain. 3D colocalization analysis was performed using Volocity 4.0 Restoration software (Volocity, Improvision). All DAB sections were examined with a Zeiss AxioObserver.Z1 inverted microscope at 10×. Sequential tile scans were performed to capture wide-field images of the whole section at 10×. Immunofluorescence images of coculture experiments were captured at 20× magnification, ten images per coverslip at either 512 × 512 resolution or 1,024 × 1,024 resolution, randomized and quantified by a technician who did not know the identity of the samples (*n* = 2 coverslips, 10 images per coverslip).

Statistical analyses and sample sizes. Statistical analyses were performed using GraphPad Prism 5.0 (Graph Pad Software, La Jolla, CA, USA) and Stata 12.1 (College Station, TX, USA). No statistical methods were used to predetermine sample sizes, but our sample sizes are similar to those previously reported²². Normality of the data and homogeneity of group variances were assessed using the Shapiro-Wilk *W* test and Levine's test respectively. When assumptions were not met or sample sizes were insufficient to test assumptions, non-parametric tests were employed. Adjustments were made for multiple testing under each hypothesis, via Bonferroni correction. Statistical significance was determined if the adjusted *P* was 0.05. Data are represented in dot plot graphs with mean ± s.e.m. To investigate tau uptake into recipient neurons via the extracellular media we measured tau levels in neurons from *MAPT*^{-/-} knock-out mice at baseline (no incubation, *n* = 4 coverslips), 1–12 h after the conditioned media were added (*n* = 6 independent coverslips), and 1–6 d after addition of conditioned media (*n* = 4 independent coverslips). A Wilcoxon rank-sum test was employed to test for differences in the levels of tau, comparing tau levels at baseline levels with levels at 6 h or less, and tau at baseline with levels at 1–6 d. To examine whether tau release is enhanced following neural activity *in vitro*, primary neurons were stimulated with picrotoxin. Levels of mouse tau in wild-type neurons (mTau) (*n* = 9 separate coverslips), mouse tau plus hTau in rTg4510 neurons (mTau + hTau) (*n* = 9 separate coverslips) and hTau in iPSC cultures (hTau) (*n* = 6 separate coverslips) was assessed. For each model, additional and independent cultures (mTau *n* = 9; mTau + hTau *n* = 9; hTau *n* = 6) were used as the nonstimulated

control group. Experiments were performed over 2 d, with 50% of the independent samples assessed on each experimental day. Samples were analyzed as a single group (regardless of experimental day), using individual Student's *t*-tests (with Satterthwaite's approximation for unequal group variance) to determine differences between control and picrotoxin treatment in the three models. *In vitro* optogenetic stimulation was performed using four separate cultures for each of three experimental conditions: control, nonstimulated ChR and simulated ChR. Differences in tau release across conditions were tested using a Kruskal-Wallis omnibus test, followed by Dunn's *post hoc* tests with a Bonferroni correction. To test the hypothesis that transfer of tau is enhanced by stimulating neuronal activity, the percent of recipient neurons with hTau from the donor was calculated (the number of cells expressing mCherry that were YFP positive/total mCherry positive cells \times 100%). For each condition (stimulated and nonstimulated), neurons were plated on $n = 5$ independent coverslips. To obtain an accurate representation of neurons across each coverslip, multiple images were used for cell counting. The percent of total neurons with tau transferred from the donor were compared between stimulated and nonstimulated conditions using a Student's *t*-test. Gene expression (**Supplementary Fig. 1**) was compared between the optogenetically stimulated side of the hippocampus (S, $n = 6$ animals) and the nonstimulated sides (NS, $n = 6$ animals), using a paired sample *t*-test. To test the hypothesis that atrophy due to stimulation would be significantly different in the tau mice ($n = 4$), as compared to tau knockout mice ($n = 4$), left and right cell body layers in the hippocampus were measured in Nissl-stained sections using ImageJ. Nissl signal above threshold levels were compared between the regions of interest on each side of the brain slice. The threshold value was kept

the same between slices within an animal. The value for the left (stimulated) hippocampus was divided by the right (nonstimulated) hippocampus to obtain a ratio of left divided by right signal in each slice. Ratios of all slices from each animal were averaged. A Wilcoxon rank-sum test was employed to compare the ratio of left/right staining across mouse groups. The Wilcoxon-rank test statistic would be expected to approximate a normal distribution with this sample size. In figures, calculated probabilities are symbolized by asterisks as follows: * $P < 0.05$; ** $P < 0.01$; *** $P < 0.001$. Optogenetic stimulation and immunofluorescent image analysis was performed by a blinded observer. Other blinded authors analyzed DAB and immunofluorescent stains of brain tissues (nonstimulated hemisphere versus stimulated hemisphere). Statistical analysis was not performed blinded to the experimental conditions. For optogenetic and chemogenetic experiments, mice of the appropriate age were selected from several different litters and randomly assigned as control or experimental. No other randomization in experimental conditions or stimulus presentations was performed.

A **Supplementary Methods Checklist** is available.

Data availability. The data that support the findings of this study are available from the corresponding author upon request. The authors declare that data supporting the findings of this study are available within the article. Source data for **Figures 4b, 5a,b,g,h, 6b** and **7h** are provided within the article.

50. Acker, C.M., Forest, S.K., Zinkowski, R., Davies, P. & d'Abramo, C. Sensitive quantitative assays for tau and phospho-tau in transgenic mouse models. *Neurobiol. Aging* **34**, 338–350 (2013).